Electronic Supplementary Information

Single-Cell-Derived Tumor-Sphere Formation and Drug-Resistance Assay Using an Integrated Microfluidics

Long Pang†‡, *Jing Ding*‡, *Yuxin Ge*†, *Jianglin Fan**†, *and Shih-Kang Fan** § ‡

† School of Basic Medical Science, The Shaanxi Key Laboratory of Brain Disorders, Xi'an Medical University, Xi'an, 710021, China.

‡ Key Laboratory of Thermo-Fluid Science and Engineering of MOE, School of Energy and Power Engineering, Xi'an Jiaotong University, Xi'an, 710049, China.

§ Department of Mechanical Engineering, National Taiwan University, Taipei, 10617, Taiwan.

* E-mail: jianglin@yamanashi.ac.jp. Phone: + 86-29-861 775 52. Fax: + 86-29-861 775 52.

* E-mail: skfan@fan-tasy.org. Phone: +886-233664515, Fax +886-223631755.

Abstract. This Supplementary Information includes all additional information as noted in the text.

Supplementary Materials and Methods

Materials and reagents. RTV 615 poly(dimethylsiloxane) (PDMS) pre-polymer and curing agent were purchased from Momentive Performance Materials (Waterford, NY, USA). Surface-oxidized silicon wafers were from Shanghai Xiangjing Electronic Technology, Ltd. (Shanghai, China), AZ 50XT photoresist and developer from AZ Electronic Materials (Somerville, NJ, USA), and SU-8 2025 photoresist and developer from Microchem (Newton, MA, USA). Fluorescein diacetate (FDA), propidium iodide (PI) and bovine serum albumin (BSA) were obtained from Sigma-Aldrich (MO, USA). The DEVD-NucView 488 Caspase-3 assay kit and the JC-1 mitochondrial membrane potential detection kit were purchased from Biotium, Inc. (Hayward, CA). Cell culture medium, fetal bovine serum (FBS) and Cell Tracker Green CMFDA were from Gibco Invitrogen Corporation (CA, USA). Vincristine was purchased from Hai zheng Pharmaceutical Co., Ltd (Zhejiang, China). The analytical reagent-grade solvents and other chemicals were purchased from local commercial suppliers, unless otherwise stated. All solutions were prepared using ultra-purified water supplied by a Milli-Q system (Millipore®).

Device fabrication. The microfluidic device utilized for this study was fabricated using the multilayer soft lithography method[1]. We designed the patterns of the device using the AutoCAD software. Generally, two different molds were first produced by photolithographic processes to create the single-cell capture channel (channel width: 400 μm, height: 25 μm; cell culture chamber width: 2 000 μm, height: 25 μm, length: 4 500 μm, respectively.) and cell culture chamber layer (length: 100 μm, width: 100 μm; height: 75 μm) embedded in the respective layers of the PDMS. To prepare the mold utilized for the fabrication of the fluidic components, a 25-μm thick positive photoresist (AZ 50XT, AZ Electronic Materials) was

spin-coated onto a silicon wafer. After UV exposure, the single-cell capture components on the wafer were developed using an AZ 400K developer (AZ Electronic Materials). To prepare the mold utilized for the fabrication of the cell culture chamber components, a 75-μm thick negative photoresist (SU8-2025, Micro. Chem.) was spin-coated onto a silicon wafer. After UV exposure, the cell culture chamber components on the wafer were developed using the SU-8 developer (Micro. Chem.).

Before fabricating the microfluidic device, both molds were exposed to trimethylchlorosilane (TMSCl) vapor for 2-3 min[1]. A well-mixed PDMS pre-polymer (RTV 615 A and B in 5 to 1 ratio) was then poured onto the fluidic mold placed in a Petri dish to yield a 2-mm thick single-cell capture channel layer. Another portion of PDMS pre-polymer (RTV 615 A and B in 15 to 1 ratio) was spin-coated onto the cell culture micro-wells to obtain the cell culture chamber layer. Two layers were cured in an 80 ^{o}C oven for 30 min. After incubation, the layers were peeled off the mold, and holes were introduced into the single-cell separation channel layer for cell and reagent access and waste exclusion. The cell culture chamber layer was then trimmed, cleaned, and aligned onto the single-cell capture channel layer with inverted microscope (Olympus, CKX41). After baking at 80 ^{o}C for 48 h, the lateral of these assembled layers was coated with PDMS pre-polymer (GE RTV 615 A and B in 10 to 1 ratio), and cured for 2 h in the oven (80 ^{o}C). The microfluidic device was ready for use after baking at 80 ^{o}C for another 48 h.

Cell culture. Human glioblastoma U251 cells were obtained from the Chinese Academy of Sciences (Shanghai, China). In this study, two different cell culture mediums were used to culture the U251 cells, which could form two types of tumor cells, *i.e.*, standard and induced U251 cells; the two types of U251 cells have different biomechanical and drug-resistant properties[2]. Specially, for the culture of the standard U251 cells, U251 cells were routinely cultured in a humidified atmosphere of 5% CO_2 at 37 ^{o}C using

Dulbecco's modified Eagle's medium (DMEM, Invitrogen, Grand Island, NY) supplemented with 10% fetal bovine serum (FBS, Invitrogen), 100 units/mL penicillin, and 100 mg/mL streptomycin. To keep cells in the exponential growth phase, they were passaged at a ratio of 1:3 every 3 day. To prepare the cells for on-chip experiment, the serum-containing culture medium (DMEM supplemented with 10% FBS) was removed and the cells were collected by centrifugation at 2 000 rpm for 10 min after washing twice with phosphate-buffered saline (PBS, 0.01 mol/L, pH 7.4) and treating with trypsin for 10 min.

For the culture of the induced U251 cells, after harvested during their exponential growth phase, the prepared standard U251 cell suspension was centrifuged at 2 000 rpm for 10 min, and then re-suspended in serum-free neural stem cell medium (SFM) containing Dulbecco's Modified Eagle Medium/F12 (DMEM/F12) (Gibco, Grand Island, NY), B27 (1×, Invitrogen, Carlsbad, CA, USA), recombinant human epidermal growth factor (20 ng/mL; Peprotech Inc., Rocky Hill, NJ, USA), basic fibroblast growth factor (20 ng/mL; Peprotech Inc.), and leukemia inhibitory factor (10 ng/mL; Chemicon, USA). The cells were seeded in 12-well plates with about 1×10^4 cells/well, and the number of cells was counted using a regular hemacytometer. Half of the culture medium was replaced every 24 h. After 5-day culture in a humidified atmosphere of 5% CO_2 at 37 ^oC, the induced U251 cells would grow close together and formed tumorspheres. Afterwords, the tumor spheres were collected through gentle centrifugation at 800 rpm for 5 min and mechanically dissociated by pipetting the mixture up and down. The cell suspension was then filtered through a 200-mesh filter to remove the remaining aggregates. The single-cell suspensions of the induced U251 cells were collected for the following on-chip experiments.

Cell sample preparation. Two types of glioblastoma cells (stanard U251 and induced U251 cells) were used to evaluate the capability of the device to separate and trap single cells with different size and

deformability. Firstly, standard U251 and induced U251 cells were cultured separately. Afterword, to facilitate the observation during cell infusion and single cell capture, these tumor cells were stained with green fluorescence dye following the method reported previously.[3] Briefly, the standard and induced U251 cells were re-suspended separately in a pre-warmed Cell Tracker Green CMFDA solution to stain for 30 min in a humidified atmosphere with 5% CO_2 at 37 ºC. Then, the tumor cells were resuspended in the cell buffer (PBS, 0.01 mol/L, PH 7.4; citric acid, 4.8 g/L; trisodium citrate, 13.2 g/L; and dextrose, 14.7 g/L) with 1% bovine serum albumin at a density of 100 000 cells/mL.[4] To evaluate the effect of cell densities on the single cell isolation efficiency, the tumor cell suspensions were respectively diluted to the density of 2 500, 5 000, 10 000, 15 000, 20 000 and 25 000 cells/mL using the previous method.[3]

Cell viability assay. Cell viability assessment was performed using the fluorescein diacetate (FDA)/propidium iodide (PI) double-staining protocol.[5] Specially, for the on-chip cell viability experiment, after removing the buffer/vincristine from the filter matrices and rinsing with PBS (10 μL/min, 10 min), the FDA/PI staining solution (10 μg/mL each in PBS) was infused from the reagent inlet into the MOAL matrices at 10 μL/min and stained for 10 min at 25 °C. For the off-chip cell viability experiment, the cell viability of two types U251 cells was just tested before on-chip single-cell isolation experiment using FDA/PI double-staining protocol.[6]

Cell proliferation. Cell proliferation assessment was performed using the 3-(4,5)-dimethylthiahiazo(-z-y1)-3,5-di-phenytetrazoliumromide (MTT) protocol.[7] For the standard U251 cells, the cells were re-suspended separately and seeded in 96-well plates at 1000 cells/well in DMEM containing 10% FBS. For the induced U251 cells, the cells dissociated from tumor spheres and adherent

non-sphere forming cells were prepared into single cell suspension and seeded in 96-well plates at 1000 cells/well in 0.1 ml DMEM containing 10% FBS. On day 0, 1, 2, 5 and 10, culture medium was removed and 0.2 ml 3-(4,5)-dimethylthiahiazo(-z-y1)-3,5-di-phenytetrazoliumromide (MTT) solution (final concentration: 0.5 mg/ml; Sigma) was added. The cells were incubated for 4 h and the medium was replaced by 0.15 ml DMSO. The plates were agitated for 15 min and the optical density of the solution in the wells was measured at 570 nm in a photometer (lQuant, Bio-TEK, USA).

Numerical simulations. To evaluate the velocity field fluctuations in the device, computational fluid dynamics (CFD) simulation was performed using ESI-CFD software (V2010.0, ESI CFD, Inc.). The simulation environment was verified for steady incompressible flows. Constant flow rates were specified at the input, and the outlet was set to a fixed-pressure boundary condition. No slip boundary condition was applied at the channel walls. FLOW module in CFD-ACE+ were used to explore the flow velocity distribution in the microchannels. Based on the finite volume method, the conservation of Navier–Stokes momentum in the device is described by the equation (Eq. S1) as follows.[4]

$$\frac{\partial}{\partial t}\left(\rho\vec{V}\right)+\nabla\cdot\left(\rho\vec{V}\vec{V}\right)=-\nabla P+\nabla\cdot\bar{\bar{\tau}} \qquad \text{(Eq. S1)}$$

The conservation of mass is described by the continuity equation (Eq. S2) as follows.

$$\frac{\partial\rho}{\partial t}+\nabla\cdot\left(\rho\vec{V}\right)=0 \qquad \text{(Eq. S2)}$$

where ρ is the fluid density, $\overrightarrow{\rho}$ is the velocity vector of the fluid, P is the pressure and $\bar{\bar{\tau}}$ is the stress tensor.

Single cell isolation and collection efficiency. For the study of single cell isolation and distribution, single cell isolation efficiency calculated using the following equation (Eq. S3).

$$Single\ cell\ isolation\ efficiency = \frac{Single\ cell\ _{matrices}}{Tumor\ cell\ _{matrices}} \times 100\% \qquad \text{(Eq. S3)}$$

Where *Single cell* $_{matrices}$ is the single cells captured in the micro-unit matrices, *Tumor Cell* $_{matrices}$ is all the cells captured in the micro-unit matrices.

The cell distribution rate in each micro-unit matrix was calculated using the following equation (Eq. S4).

$$Cell\ distribution\ rate = \frac{Tumor\ cell\ _{matrix}}{Tumor\ cell\ _{matrices}} \times 100\% \qquad \text{(Eq. S4)}$$

where *Tumor Cell* $_{matrix}$ is the cells captured in each micro-unit matrix, *Tumor Cell* $_{matrices}$ is the cells captured in all the micro-unit matrices.

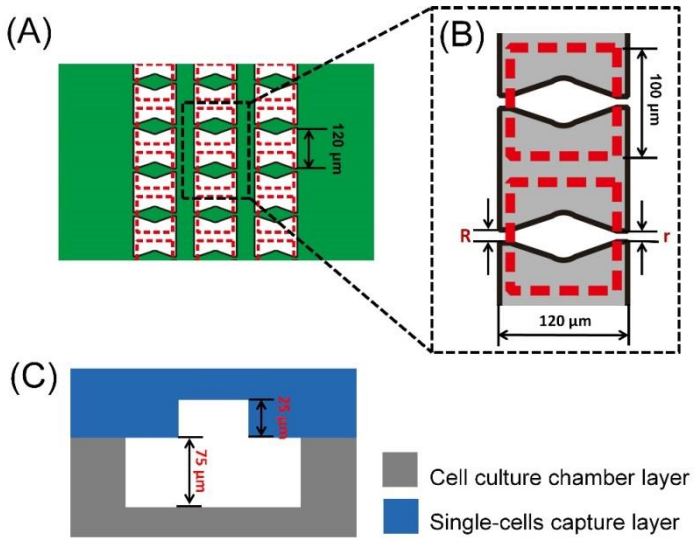

Figure S1. Schematic diagram of one micro-unit matrix. (A) Schematic diagram of the top view of one micro-unit matrix. Each matrix in the device is composed of 3 columns and many rows (from input to output of the device the rows are 45, 45, 48, 48 and 48, respectively). (B) One multi-obstacle architecture-looking (MOAL) filter composed of two neighbouring I-shaped microstructures and corresponded to a micro-well for single-cell capture and culture. For each filter, the first pore size (R) is 2 μm larger than the second pore size (r). (C) Schematic diagram of the lateral view of one multi-obstacle architecture-looking filter matrix. For each micro-well, the length, width and height is 100 μm, 100 μm and 75 μm, respectively.

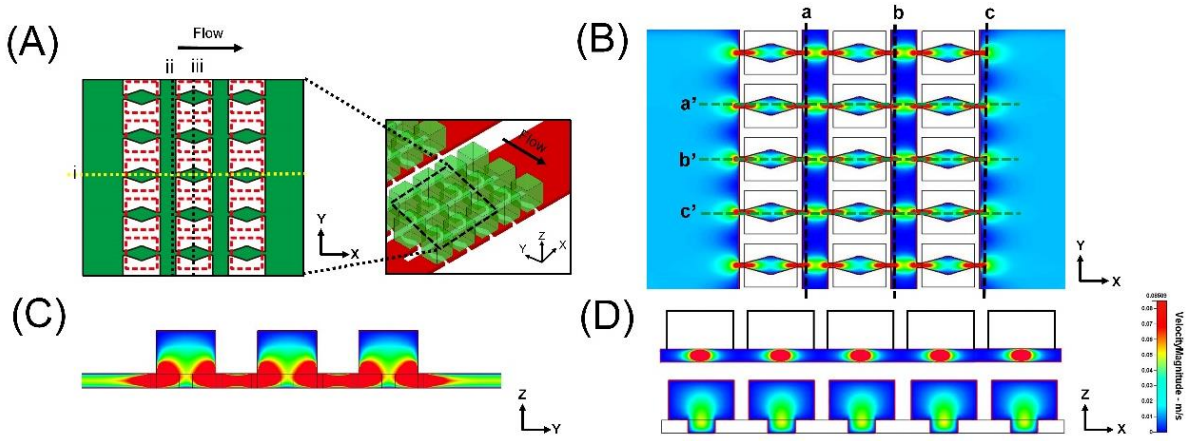

Figure S2. Computational simulation of the fluid velocities in the 10-μm micro-unit matrix (*i.e.,* the second pore size of the MOAL filter matrix is 10 μm) at the flow rate of 40 μL/min (the velocity magnitude is 0.015 m/s). (A) Schematic diagram of the design in 10-μm micro-unit matrix of the microdevice. The various channels are shown in different colors to help to distinguish the different components of the microfluidic device. Green indicates the single-cell culture chamber array and red indicates single-cell capture channels. (B) Simulated demonstration of the fluid velocities corresponding to the positions in (A), the dotted lines (a, b, c, a', b' and c') were used to analyze the fluid velocity distributions in the 10-μm filter matrix. (C) Simulated demonstration of the fluid velocities corresponding to the yellow dotted line(i) in (A). (D) Simulated demonstration of the fluid velocities corresponding to the black dotted lines (ii and iii) in (A) from left to right is(ii) and (iii), respectively.

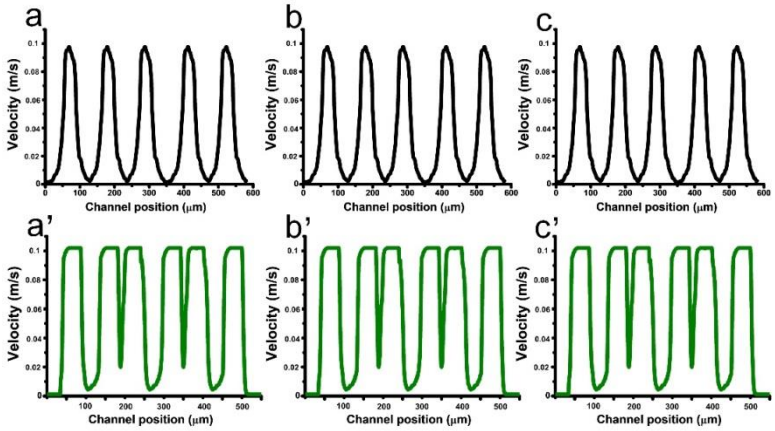

Figure S3. Quantitative analysis of the fluid velocities in the 10-μm micro-unit matrix at the velocity magnitude of 0.018 m/s, which correspond to the positions of the dotted lines (a, b, c, a', b' and c') in **Figure S2 (B)**, respectively.

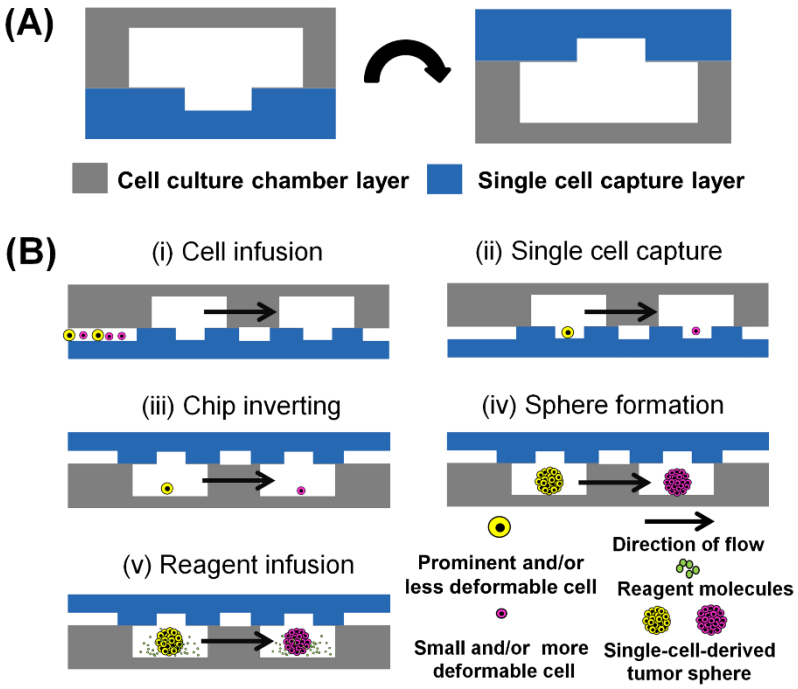

Figure S4. (A) Schematic diagram of the lateral view of single-cell separation, sphere formation and reagent infusion in the microfluidic device, which also showed that the device consisted of two layers: cell culture chamber layer, single cell capture layer. (B) Schematic diagrams showing the operation of cell infusion, single cell capture, sphere formation and reagent infusion. During the cell infusion and single cell capture steps, the filter matrices allow the cell sample could be sorted according to their size and deformability. During the chip inverting and sphere formation phases, the chip was inverted to download the trapped single cells into the micro-wells from the MOAL filter microstructural matrices. During the reagent infusion phase, reagents were loaded for co-culture of tumor-spheres at different treatment times.

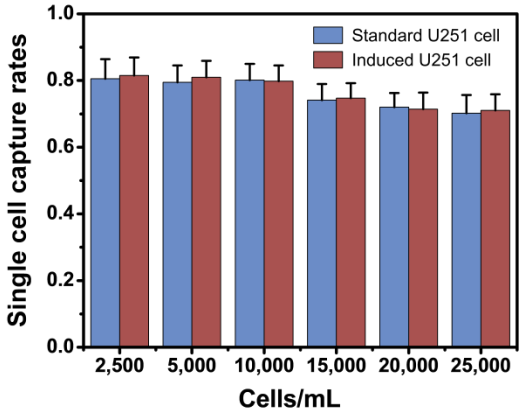

Figure S5. The isolation efficiency of the single cells in the device under different cell densities, indicating that the single cell isolation efficiency at low cell densities (2 500, 5 000, and 10 000 cells/mL) are higher than those at the high cell densities (15 000, 20 000, 25 000 cells/mL), that is $p < 0.05$. And the single cell isolation efficiency between the two types of U251 cell (the standard and induced U251 cell) at the same cell densities is not significant. The infusion flow rate is 40 μL/min. The standard deviations deduced from ten parallel experiments are shown as the error bars. The significance assessed by ANOVA from ten parallel experiments.

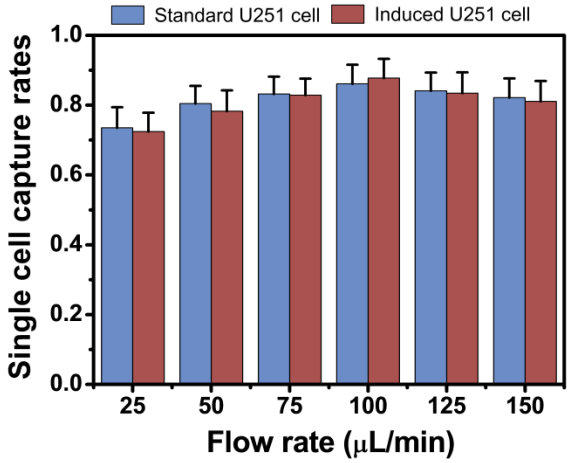

Figure S6. The isolation efficiency of single cells in the device under different infusion flow rates, indicating that the single cell isolation efficiency at 100 μL/min are higher than those at the other infusion flow rates (25, 50, 75, 125 and 150 cells/mL), that is $p < 0.05$. And the single cell isolation efficiency between the two types of U251 cell (the standard and induced U251 cell) at the same infusion flow rates is not significant. The cell density is 10 000 cells/mL. The standard deviations deduced from ten parallel experiments are shown as the error bars. The significance assessed by ANOVA from ten parallel experiments.

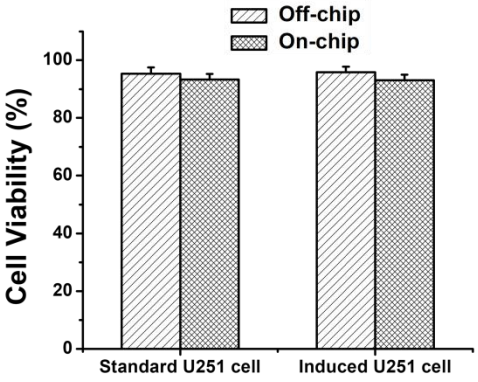

Figure S7. Quantitative analysis of the on- and off-chip cell viability by using FDA/PI double-staining protocol, indicating that the single cells captured in the device remain highly viable, similar to off-chip cultured cells, retrieving >93% viable cells. Standard deviations deduced from ten parallel experiments were shown as the error bars.

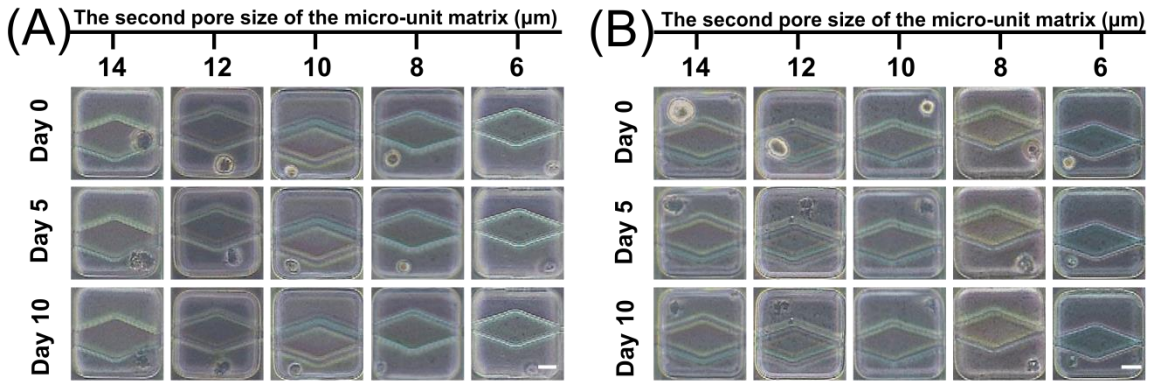

Figure S8. Microscopic images of cells in single standard (A) and induced (B) U251 cell-derived assay in different micro-unit matrices of the device. Non-stem-like cells died of anoikis due to the loss of anchorage. The sizes of the micro-unit matrices are the sizes of the second pores in each MOAL filter matrix. (scale bar: 25 μm).

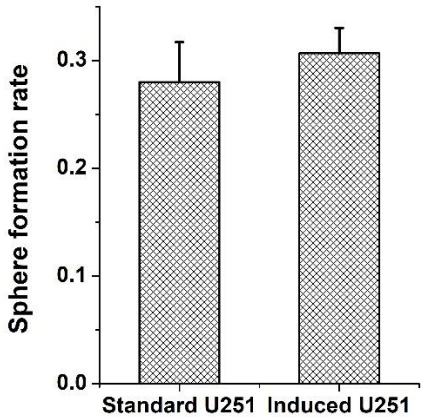

Figure S9. Statistical sphere formation efficiency of the single standard and induced U251 cells in the device. Standard deviations deduced from ten parallel experiments were shown as the error bars.

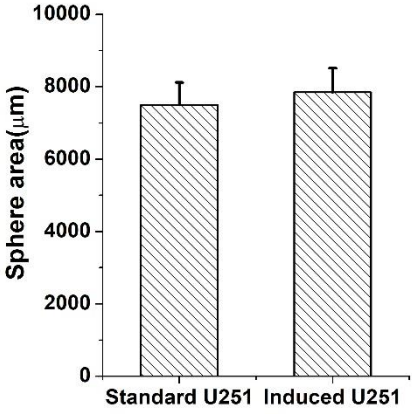

Figure S10. Statistical sphere area of the single standard and induced U251 cell-derived sphere in the device. Standard deviations deduced from ten parallel experiments were shown as the error bars.

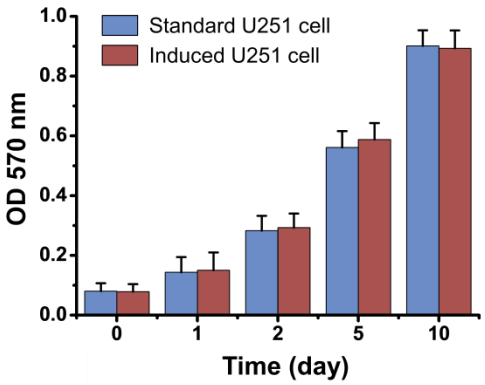

Figure S11. Comparison of growth state of standard and induced U251 cells by reseeding cells back into culture. Standard deviations deduced from ten parallel experiments were shown as the error bars.

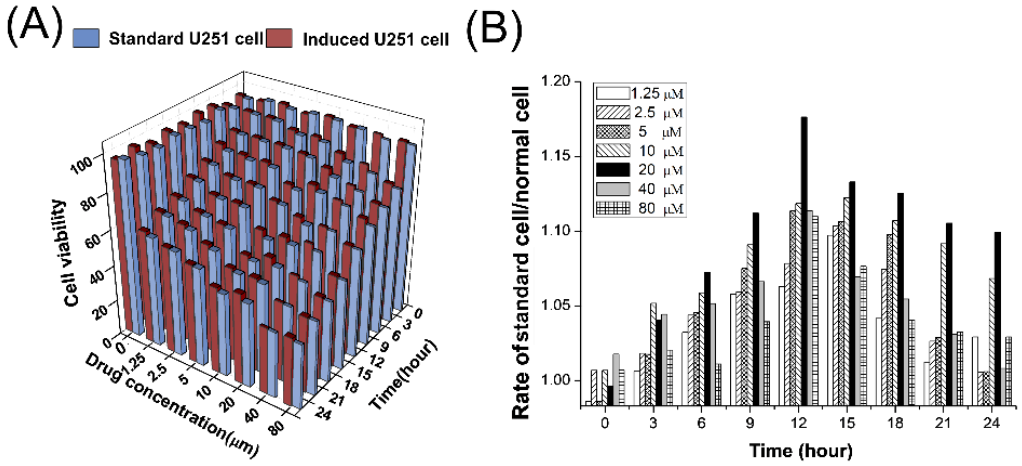

Figure S12. (A) The statistical cell viability of single-cell-derived sphere after different time and vincristine concentration treatments. (B) The ratios of the cell viabilities in single induced/standard U251 cell-derived sphere were used to reflect the quantitative dynamics of the cell viability during chemotherapy, corresponding to (A).

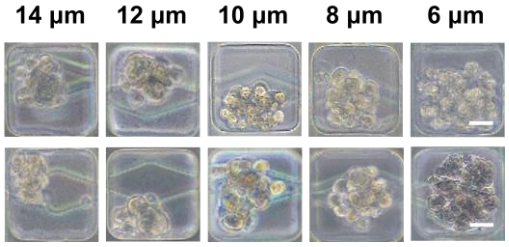

Figure S13. The viability assay of the single-cell-derived sphere in different micro-unit matrices after 12-hour treatment with 20 μM vincristine. The first row showed the bright-field image of the single standard U251 cell-derived sphere. The second row showed the bright-field image of the single induced U251 cell-derived sphere. Fluorescence image of the single standard and induced U251 cells derived sphere in the micro-unit matrices after vincristine treatment were shown in **Figure 4A**. The sizes of the micro-unit matrices are the sizes of the second pores in each MOAL filter matrix (scale bar: 25 μm).

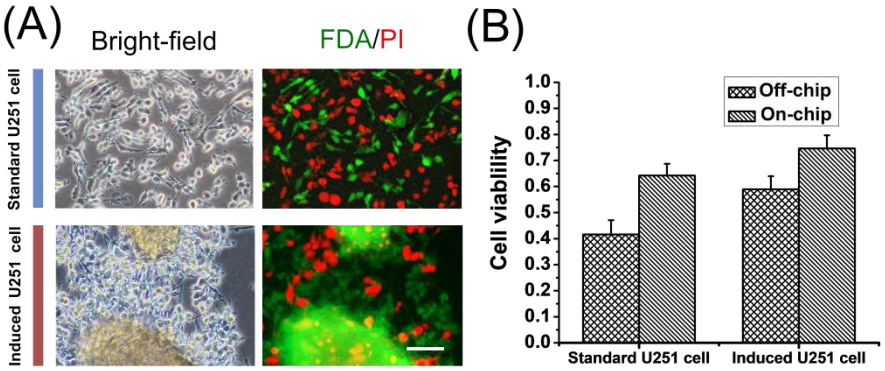

Figure S14. Comparison of the on- and off-chip cell viabilities after 12 hours treatment with 20 μM vincristine. (A) The bright-field (left) and fluorescence (right) images of the off-chip (control) standard (the first row) and induced (the second row) U251 cells. (B) Quantitative analysis of cell viabilities of the on and off-chip U251 cells. The results confirmed that the on-chip cell viability is similar to the off-chip (control) cells. Scale bars, 100 μm. Standard deviations deduced from ten parallel experiments were shown as the error bars.

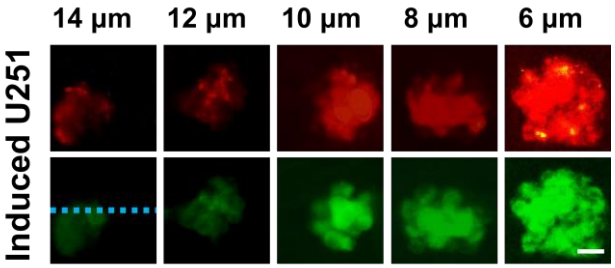

Figure S15. Fluorescence images using JC-1 aggregate (red) and monomer (green) in single-cell-derived sphere in different micro-unit matrices of the device without vincristine treatment. Fluorescence image of the standard U251 cells captured in the micro-unit matrices was shown in **Figure 4C**. The sizes of the micro-unit matrices are the sizes of the second pores in each MOAL filter matrix (scale bar: 25 μm).

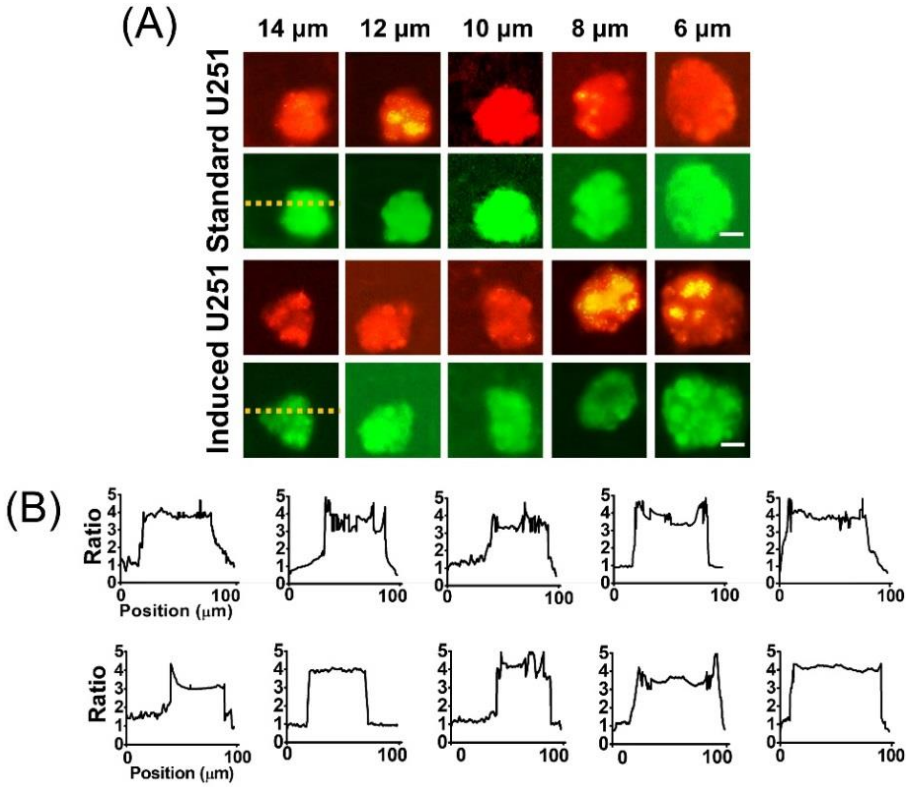

Figure S16. Mitochondrial membrane potential of in standard and induced U251 cells in single-cell-derived sphere in different micro-unit matrices of the device without vincristine treatment. (A) Fluorescence images using JC-1 aggregate (red) and monomer (green) of standard and induced U251 cells in single-cell-derived assay in different micro-unit matrices of the device without vincristine treatment, the scale bars in (A) represent 25 μm. (B) Statistical ratio of JC-1 aggregate to its monomeric form in standard (the first row) and induced U251 cells (the second row) without vincristine treatment. The sizes of the micro-unit matrices are the sizes of the second pores in each MOAL filter matrix.

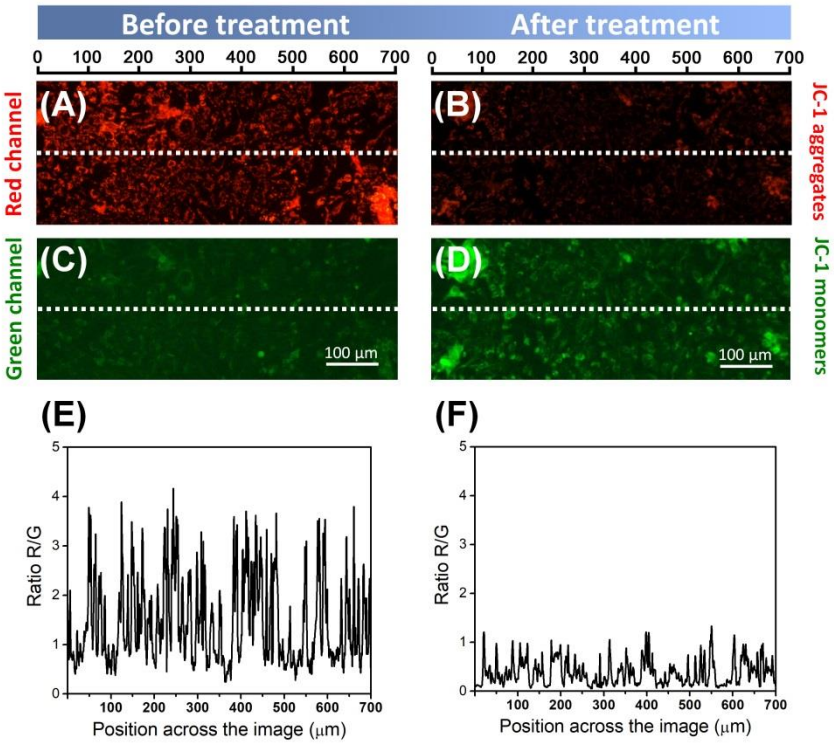

Figure S17. Mitochondrial membrane potential of the standard U251 cells cultured using the conventional plate-based method. (A and B) Fluorescence images of JC-1 aggregates in the mitochondria of standard U251 cells before (A) and after (B) 12 h treatment with 20 μM vincristine. (C and D) Fluorescence images of JC-1 monomers in the cytoplasm of standard U251 cells before (C) and after (D) 12 h treatment with 20 μM vincristine. (E and F) Ratios of JC-1 aggregate to its monomer before (E) and after (F) 12 h treatment with 20 μM vincristine, corresponding to the dotted lines in (A) and (C), as well as (B) and (D), respectively.

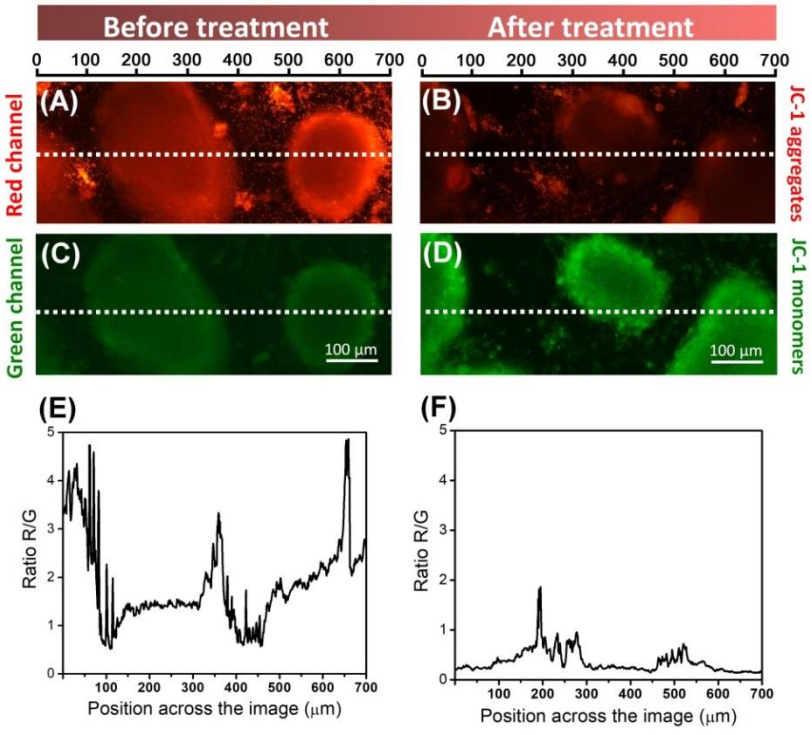

Figure S18. Mitochondrial membrane potential of the induced U251 cells cultured using the conventional plate-based

method. (A and B) Fluorescence images of JC-1 aggregates in the mitochondria of induced U251 cells before (A) and after (B) 12 h treatment with 20 μM vincristine. (C and D) Fluorescence images of JC-1 monomers in the cytoplasm of induced U251 cells before (C) and after (D) 12 h treatment with 20 μM vincristine. (E and F) Ratios of JC-1 aggregate to its monomer before (E) and after (F) 12 h treatment with 20 μM vincristine, corresponding to the dotted lines in (A) and (C), as well as (B) and (D), respectively.

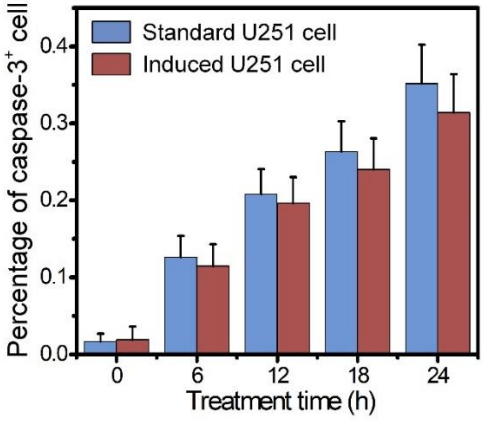

Figure S19. On-chip caspase-3 activation (capase-3^+) of in single standard and induced U251 cell-derived sphere in the micro-unit matrices of the device after different time treatments with 20 μM vincristine. Standard deviations deduced from ten parallel experiments were shown as the error bars.

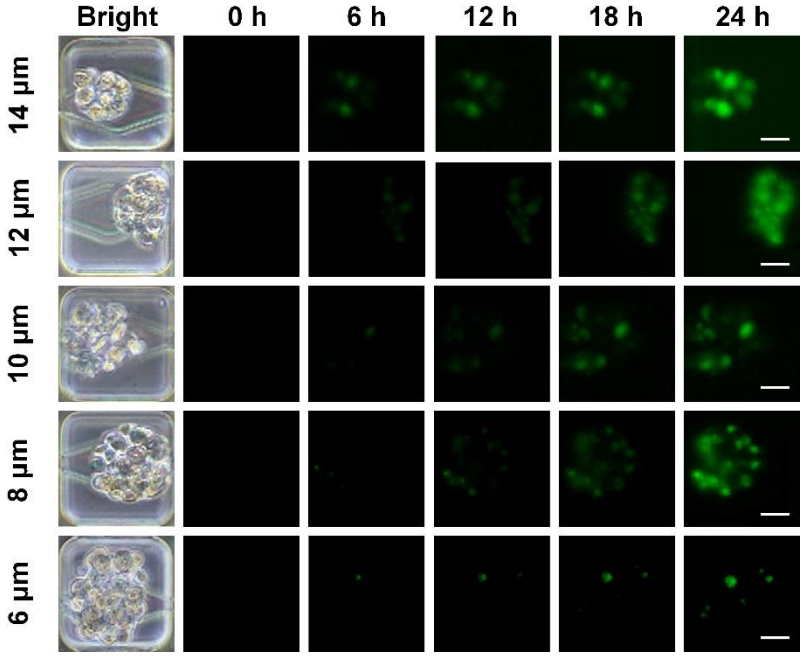

Figure S20. Caspase-3^+ cells in single standard U251 cell-derived sphere in the micro-unit matrices of the device after different time treatments with 20 μM vincristine. Temporal fluorescence images of the caspase-3^+ cells in single standard U251 cell-derived sphere in the micro-unit matrices after different time treatments with 20 μM vincristine. The Bright-field of standard U251 cells before 20 μM vincristine treatment is shown in the first column. The sizes of the micro-unit matrices are the sizes of the second pores in each MOAL filter matrix. Scale bars are 25 μm.

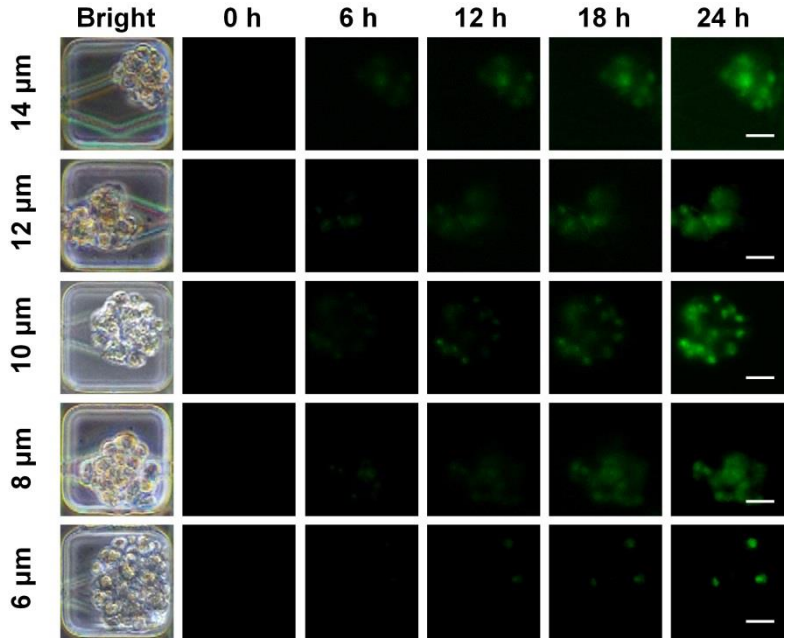

Figure S21. Caspase-3^{+} cells in the single induced U251 cell-derived spheroid in the micro-unit matrices of the device after different time treatments with 20 μM vincristine. Temporal fluorescence images of the caspase-3^{+} cells in single induced U251 cell-derived sphere in the micro-unit matrices after different time treatments with 20 μM vincristine. The Bright-field of induced U251 cells before 20 μM vincristine treatment is shown in the first column. The sizes of the micro-unit matrices are the sizes of the second pores in each MOAL filter matrix. Scale bars are 25 μm.

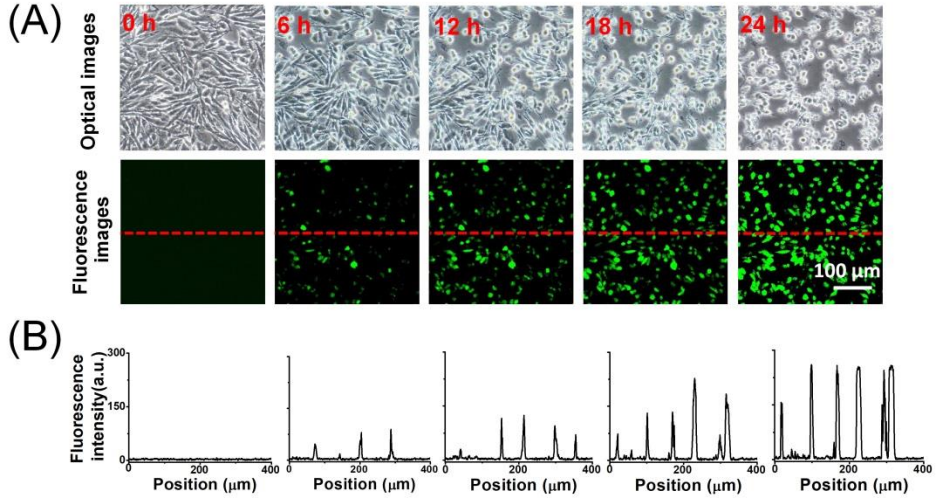

Figure S22. Off-chip caspase-3 activation of the standard U251 cells after different time treatments with 20 μM vincristine. (A) Fluorescent images of caspase-3^{+} standard U251 cells after different time treatments with 20 μM vincristine. (B) Fluorescence intensity distribution of the caspase-3^{+} cells at various treatment times (from left to right: 0, 6, 12, 18, 24 h, respectively), corresponding to the dotted line in (A).

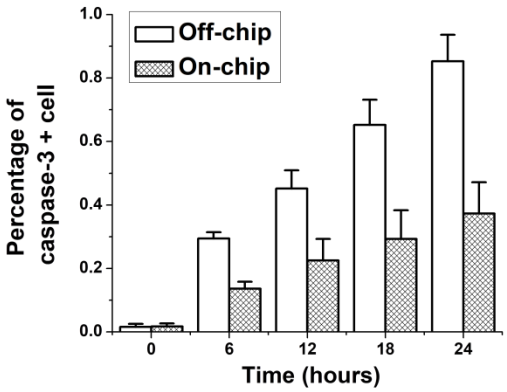

Figure S23. Quantitative percentages of the caspase-3$^+$ standard U251 cells after on- and off-chip vincristine treatments. Standard deviations deduced from ten parallel experiments were shown as the error bars.

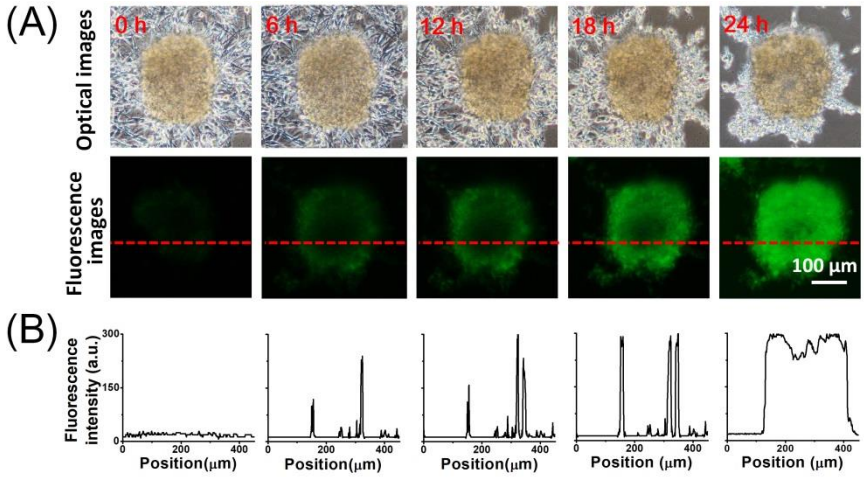

Figure S24. Off-chip caspase-3 activation of the normal U251 cells after different time treatments with 20 μM vincristine. (A) Fluorescent images of caspase-3$^+$ normal U251 cells after different time treatments with 20 μM vincristine. (B) Fluorescence intensity distribution of the caspase-3$^+$ cells at various treatment times (from left to right: 0, 6, 12, 18, 24 h, respectively), corresponding to the dotted line in (A).

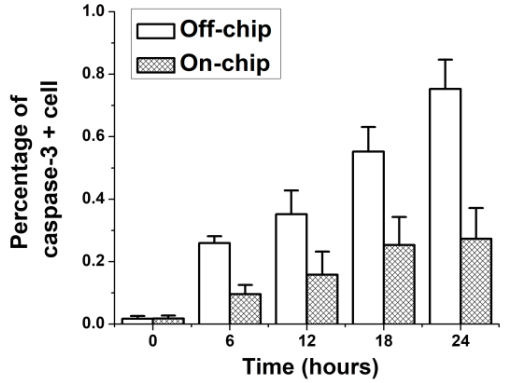

Figure S25. Quantitative percentages of the caspase-3$^+$ induced U251 cells after on- and off-chip vincristine treatments. Standard deviations deduced from ten parallel experiments were shown as the error bars.

References for the ESI.

(1) J. Y. Wang, G. D. Sui, V. P. Mocharla, R. J. Lin, M. E. Phelps, H. C. Kolb and H. R. Tseng, *Angewandte Chemie-International Edition*, **2006**, 45, 5276-5281.

(2) X. Q. Wang, F. Wei, A. J. Liu, L. Wang, J. C. Wang, L. Ren, W. M. Liu, Q. Tu, L. Li and J. Wang, *Biomaterials*, **2012**, 33, 3719-3732.

(3) S. F. Shen, C. Ma, L. Zhao, Y. L. Wang, J. C. Wang, J. Xu, T. B. Li, L. Pang and J. Wang, *Lab Chip*, **2014**, 14, 2525-2538.

(4) L. Pang, S. F. Shen, C. Ma, T. T. Ma, R. Zhang, C. Tian, L. Zhao, W. M. Liu and J. Wang, *Analyst*, **2015**, 140, 7335-7346.

(5) L. Ren, W. M. Liu, Y. L. Wang, J. C Wang, Q. Tu, J. Xu, R. Liu, S. F. Shen and J. Wang, *Anal. Chem.*, **2013**, 85, 235-244.

(6) W. M. Liu, J. Xu, T. B. Li, Y. L. L. Zhao, C. Ma, S. F. Shen and J. Wang, *Anal. Chem.*, **2015**, 87, 9752-9760.

(7) S. C. Yu, Y. F. Ping, L.Yi, Z. H. Zhou, J. H. Chen, X. H. Yao, L. Gao, J. M. Wang. and X. W. Bian,. *Cancer lett*., **2008**, 265, 124-134.